

# Modeling Fluid Mixing in Microfluidic Grids

**Huong Luu**

Department of Computer Science  
University of California at Riverside

**Marek Chrobak**

Department of Computer Science  
University of California at Riverside

---

## Abstract

We describe an approach for modeling concentration profiles in grid-based microfluidic chips for fluid mixing. This approach provides an algorithm that accurately predicts fluid concentrations at the chip outlets. Our algorithm significantly outperforms COMSOL finite element simulations.

**2012 ACM Subject Classification** Applied computing → Physical sciences and engineering • Emerging technologies → Emerging simulation

**Keywords and phrases** algorithms, graph theory, lab-on-chip, fluid mixing

**Digital Object Identifier** 10.4230/LIPIcs...

**Funding** Research supported by NSF grant CCF-1536026.

## 1 Introduction

Microfluidics is an emerging technology for manipulating nanoliter-scale fluid volumes, with applications in a variety of fields including biology, chemistry, biomedicine, or materials science. Fast progress in this area led to the development of microfluidic chips (MFCs), which are integrated microfluidic devices that are increasingly used in various laboratory processes such as medical diagnosis [15], DNA purification [9], cell lysis [8], and other. MFCs offer a solution to automate laboratory experiments that saves time, reduces labor costs, limits usage of chemical reagents, and replaces complex and expensive equipment [12, 8].

One function often implemented on MFCs is fluid mixing. This function is particularly important in its application in sample preparation, where the objective is to dilute the sample fluid, also called *reactant*, using another fluid that we refer to as *buffer*. For example, in cell lysis, sample preparation process includes a step of mixing blood sample with citrate buffer [8]. For some experimental processes multiple diluted samples are sometimes needed, with desired volumes and concentrations. For example, an experimentation process may involve a sample consisting of  $5\mu L$  of reactant with concentration 10%,  $10\mu L$  of reactant with concentration 20%, and  $10\mu L$  of reactant with concentration 40%. Samples involving multiple concentrations are common in preclinical drug development processes. One other application where multiple target concentrations of the same reactant are commonly used is in biochemical assays [3].

The MFC solutions for dilution chips proposed so far fall into two different categories: droplet-based chips, where the fluid is manipulated in discrete units called droplets, and flow-based chips, based on continuous flow.

In our work we focus on the flow-based model. Several flow-based designs have been proposed in the literature. In [11], the authors proposed an MFC that uses two-way valves to produce serial dilution. An electrokinetically driven MFC design was introduced in [6] for serial mixing. The above approaches require different design by changing valves or splitter



© The copyright is retained by the authors;  
licensed under Creative Commons License CC-BY

Leibniz International Proceedings in Informatics

LIPICs Schloss Dagstuhl – Leibniz-Zentrum für Informatik, Dagstuhl Publishing, Germany

channels placement, or tuning voltage control to create different target sets. In [4], the authors gave a dilution algorithm for given target concentration ratios using rotary mixers. However, their method produces waste and it also uses valves which can complicate the fabrication process.

**Grid mixers.** A very different approach was developed by Wang *et al.* [14]. Their proposed solution involves creating a library of ready-to-use micromixers that users can query to find a chip design with desired properties. Their MFCs are simple rectilinear grids with no valves, two inputs (one for reactant and one for buffer) and three outlets, thus capable of producing a set of three different concentrations. A user identifies an appropriate design by submitting a query consisting of the desired reactant concentrations. In their approach the design process is eliminated and the database is created by exploring a large collection of randomly generated grids. For each random grid, its outlet concentration values are computed by simulating fluid flow through the grid using COMSOL Multiphysics® software (a commercial software that uses finite element analysis method to model physics processes, including fluid dynamics). As shown in [14], these COMSOL simulation results provide very accurate prediction of outlet concentrations in actual fabricated MFCs.

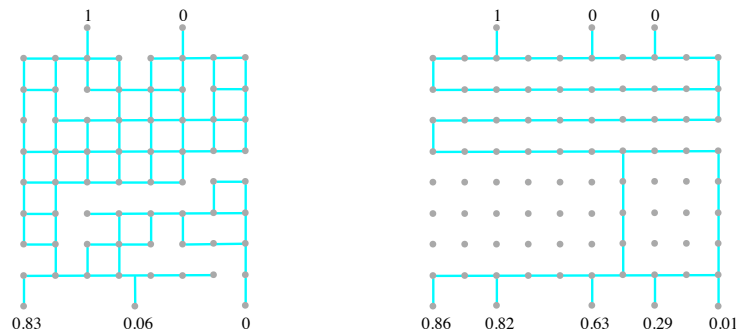
Exploring such random designs is extremely time consuming, as most randomly generated designs are actually not useful, either because they are redundant or because they produce concentrations that are of little interest (for example, only near-pure reactant or buffer). Thus to produce a desired number of designs for the grid library, one may need to examine orders of magnitude more random designs.

With the need to test so many designs, this approach can only be used for small size grids because of the simulation bottleneck of COMSOL Multiphysics®. The simulation time for each design in [14] is roughly a minute. It is also not scalable to bigger grids. COMSOL Multiphysics® can take up to 6 minutes to run a simulation for  $12 \times 12$  grid with the same mesh setting. The process can be sped up by using a coarser mesh, but with the cost of loss of outlet accuracy. Further, some users may prefer to design custom grids for their choices of the attributes: velocity, solute, outlets' locations, diffusion coefficient of reactant, etc. Such users would need to have access to an often costly CFD (Computational Fluid Dynamic) software in order to be able to run the simulations.

The approach based on random grid generation was also considered in [7], where the authors propose a method to remove redundant channels to make the design process more efficient, simplifying fabrication of grid MFCs and reducing reactant usage.

**Our contribution.** Addressing this performance bottleneck in populating the grid library in the approach from [14], we developed an algorithm to model fluid mixing in microfluidic grids, in order to predict the reactant concentrations at the outlets. In our approach, concentration profiles in grid channels are approximated using a simple 3-piece linear function, which allows us to simulate the mixing process in time linear in the grid size. The overall algorithm is scalable and simple, and produces good approximation of concentration values and flow rates at outlets in grid-based microfluidic chips, as compared to the results from COMSOL Multiphysics®. It is also much more general than the model from [14, 7], as it allows grids of all sizes, any number of outlets, arbitrary inflow velocities, and arbitrary fluids. We also developed a web-based implementation of our algorithm that allows users to customize their designs manually to match their needs.

While the main objective of this work was to develop an efficient numerical simulation algorithm, it also involves interesting combinatorial and topological aspects, as the correctness of our profile concentration model relies critically on duality properties of planar acyclic digraphs.



■ **Figure 1** On the left, an example of an 8x8 grid from [14]. On the right, an example of a 10x8 grid in our model, with 3 inlets and 5 outlets. The numbers at the outlets show the reactant concentrations.

## 2 Statement of the Problem

We study grid-based MFCs for fluid mixing that were introduced in [14]. Their chosen model is  $8 \times 8$  grid that has 2 inlets along the top edge of the grid (the left inlet contains reactant, with concentration value 1, and the right inlet contains buffer, with concentration value 0) and 3 outlets at the bottom, as shown in Figure 1. The channel width is 0.2 mm, and the channel length (distance between two grid vertices) is 1.5 mm. The fluid velocity in the inlets is 10 mm/s. The outlets pressure is 0 Pa. The reactant is either sodium, fluorescein or bovine serum albumin.

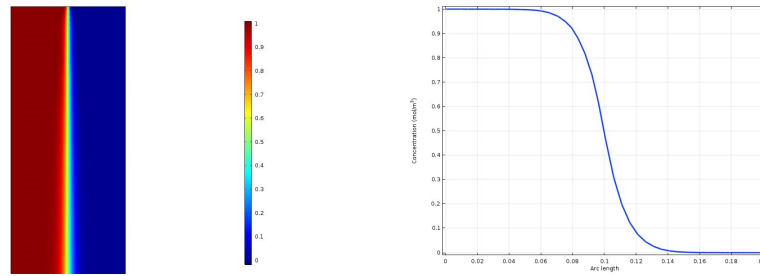
We generalize the model from [14] in several ways. We allow arbitrary  $m \times n$  grids, with any number of inlets and outlets (see Figure 1). The inlets are located along the top edge of the grid and the outlets at the bottom. The inlets' solutions can take any concentration from 0 to 1, but they must satisfy the following *inlet monotonicity property*: the inlet concentrations need to be non-increasing from left to right. The inflows are of given constant rate, and the pressure value at all outlets is 0. Our model assumes that the flow throughout the grid is laminar, which is the case in standard microfluidic applications.

## 3 Overview of the Algorithm

Our algorithm for predicting reactant concentrations at the output channels is based on modeling concentration profiles in grid's channels. Such concentration profile is a function that represents the concentration of the reactant along a line perpendicular to the channel. When fluid flows through straight segments of the grid, this profile changes according to the laws of diffusion. In a node of the grid, a flow may be split or several flows may be joined, and the profile changes accordingly producing complex non-linear functions. The main idea behind our algorithm is to approximate this profile using a simple 3-piece linear function. Once the profile at an output channel is computed, it determines the reactant concentration at this channel.

We now give an overview of our algorithm. The input consists of the grid design (including channel width and length), flow velocity and concentration values at the inputs, and the fluid's diffusion coefficient. Below we show the main steps of the algorithm, with more detailed descriptions given in the sections that follow.

- (1) Verify the correctness of the grid design, namely whether each edge (channel) is on



■ **Figure 2** The picture on the left shows the result of mixing of reactant (red) and buffer (blue) due to diffusion over some period of time. The figure on the right is a graph representing the concentration profile of this mixture.

at least one path from a source to a sink channel. (In our implementation, spurious fragments of the grid are automatically removed.)

- (2) Compute the flow rates at each channel and pressure values at the nodes (see Section 5).
- (3) Partition the grid into parts, each part being either a straight channel or a node. Depending on flow direction, a node can be one of three types: a join node (2-way or 3-way), a split node (2-way or 3-way), or a combined join/split node (with 2 inflows and 2 outflows). Sort these parts in an order consistent with the flow direction. (Once the flows are computed, one can think of the grid design as an acyclic directed graph. The desired order is then any topological sort of this acyclic graph.)
- (4) Process the grid parts, in the earlier determined order, computing approximate concentration profiles (see Section 6):
  - For a straight channel, the concentration profile at the end of the channel is determined from the profile at the beginning of the channel, based on the time the flow spends in this channel (this time is computed from the channel length and flow velocity).
  - For nodes representing flow splits, split the incoming profile into outgoing profiles according to flow velocities.
  - For nodes representing flow joins, join the incoming profiles into the outgoing profile according to the flow velocities. This outgoing profile is then approximated by a 3-piece linear function.
- (5) Once all flow profiles in the grid are determined, for each outlet channel compute its fluid concentration as the integral of its concentration profile divided by the channel width.

**Running time.** The algorithm for profile computations takes only constant time to update the profile for each node and channel, thus the overall running time is linear with respect to the size of the grid design. (Thus never worse than  $O(mn)$  for an  $m \times n$  grid.) The overall running time is thus dominated by solving the linear system in part (2). For grid sizes that might be of use in grid libraries, say up to  $20 \times 20$ , Gaussian elimination is sufficiently fast. (For large grids, one can take advantage of the sparsity of the linear systems to speed up the computation.)

#### 4 Concentration Profile Model

**True concentration profiles.** Consider a mixture of two fluids, one reactant (with concentration 1) and the other buffer (with concentration 0), flowing along a straight channel

of some width  $w$  and length  $l$ . For any fixed distance  $l' \leq l$  from the beginning of this channel, a *concentration* profile at  $l'$  is a function that gives concentrations of all points in the channel along the line segment (of length  $w$ ) that is perpendicular to the channel and directed counter-clockwise to the flow.

Figure 2 shows an example. Reactant and buffer are injected into a straight channel at the same rate and allowed to mix while they flow. Initially the profile will be a 1/0 function. The flow is assumed to be laminar and the two fluids will gradually mix as a result of diffusion. After a period of time, this mixing produces a non-uniform concentration shown in Figure 2 on the right. This concentration profile is a smooth curve with the leftmost region having concentration 1, the rightmost region having concentration 0, and the middle region contains partially mixed fluids with concentration decreasing from left to right. Using the diffusion model, this profile function can be determined from the mixing time, which is the time it takes for the fluid to flow through the channel. The width of this middle region is referred to as diffusion length and denoted  $L$  (normal to the flow direction, units  $m$ ). It can be computed from the formula (see [10]):

$$L = 2\sqrt{Dt}. \quad (1)$$

where  $t$  is the mixing time and  $D$  is the diffusion coefficient of the fluid (units  $m^2/s$ ).

In microfluidic grids the flow may be repeatedly split or different flows may get combined, and the resulting concentration profile will not have the form in Figure (2) anymore; in fact, the profile functions that arise are too complex to be captured analytically. Below we prove, however, that in our grids these profiles have a certain monotonicity property that will allow us to approximate them by a simpler function. Interestingly, this monotonicity property involves the concept of the partial order that is dual to the flow pattern.

**Concentration monotonicity property.** The intuition behind the monotonicity property is illustrated in Figure 2; intuitively, the profile function in a channel should be monotonely decreasing from left to right. This property is trivial if we start with a 1/0 profile (with pure reactant to the left of pure buffer) at the top of a vertical channel and allow the fluid to diffuse when it flows down along the channel. But in a complex grid the flow pattern may be quite complex. In a vertical channel, the flow direction could be either down or up, for example. Thus even the notions of “left” and “right” are not well defined anymore. Joins and splits complicate this issue even more.

Thus, to define this monotonicity property, we need to capture the notion of “left-to-right direction” not only with respect to one channel, but also between different channels. This notion will be formalized using a partial ordering of the grid’s channels. This partial order is defined as the dual order of the flow pattern in the grid. Below we formalize these concepts.

Once the flow directions are computed, the flow pattern through the grid design can be naturally represented as a straight-line planar drawing of a DAG (directed acyclic graph) whose nodes are the grid points (including inlets and outlets) and edges are channels with directions determined by the flow. We will denote this graph by  $G$ .

Next, we construct a dual DAG  $\tilde{G}$ . To this end, enclose the grid in a rectangle, slightly wider than the grid, with the inflows on its top edge and outflows on its bottom edge, as in Figure 5. The grid (that is, the embedding of  $G$ ) partitions this rectangle into regions. For each region of  $G$ , we create a vertex of  $\tilde{G}$ . Two vertices  $\phi, \psi$  of  $\tilde{G}$  are connected by an edge if the boundaries of their corresponding regions share at least one edge of  $G$ . The direction of the edge between  $\phi$  and  $\psi$  is determined as follows: pick any edge  $(u, v)$  of  $G$  shared by the regions of  $\phi$  and  $\psi$ . This edge  $(u, v)$  must have a different orientation in the boundaries of  $\phi$  and  $\psi$  (clockwise in one and counterclockwise in the other). Then this dual

edge between  $\phi$  and  $\psi$  is directed from the node where  $(u, v)$  is clockwise to the node where it is counterclockwise. This definition does not depend on the choice of  $(u, v)$ . We will refer to this edge as being dual to  $(u, v)$ . It can be shown that  $\tilde{G}$  is a DAG with a unique source  $\tilde{s}$  and unique sink  $\tilde{t}$  that correspond to the regions to the left and right of the grid design, respectively. (Except for secondary technical differences, the construction of such a dual can be found, for example, in [13, 2].)

We now use  $G'$  to define a partial order on the edges of  $G$  (that is, the channels of our grid design). Call two edges  $e, e'$  of  $G$  *related in  $G$*  if they are both on the same inlet-to-outlet path; otherwise call them *unrelated in  $G$* . If  $e$  and  $e'$  are unrelated in  $G$  then, denoting by  $\phi$  and  $\phi'$  their dual edges, there is a path from  $\tilde{s}$  to  $\tilde{t}$  in  $\tilde{G}$  that contains  $\phi$  and  $\phi'$ . If  $\phi$  is before  $\phi'$  on this path, then we write  $e \preceq e'$ , and say that  $e$  *dually precedes*  $e'$ . It is not difficult to verify that relation “ $\preceq$ ” is a partial order on  $G$ 's edges.

► **Theorem 1.** (*Concentration profile monotonicity.*) Consider a grid design as described in Section 2 (in particular, the inlet concentrations are non-increasing) with some flow, and its corresponding graph  $G$ . The concentration profiles in  $G$  satisfy the following properties:

(cpm1) For any edge of  $G$ , its concentration profile is a non-increasing function.

(cpm2) For any two edges  $e, e'$  of  $G$ , if  $e \preceq e'$  then all concentrations in the profile for  $e$  are at least as large as all concentrations in the profile for  $e'$ .

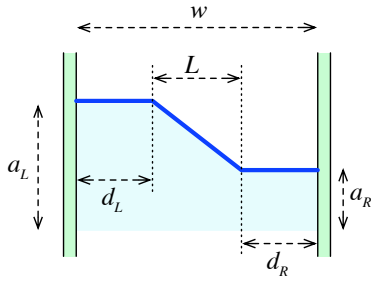
**Proof.** (Sketch.) A formal proof of Theorem 1 is omitted here; we only give a brief sketch. Define a cut  $(S, T)$  of  $G$  in a natural way, as the partition of its vertices such that each inlet-to-outlet path visits vertices in  $S$  before visiting vertices in  $T$ . We prove by induction on  $|S|$  that all edges with an endpoint in  $S$  satisfy the theorem. This is true in the base case, when  $S$  contains only inlets. In the inductive step, we move one vertex  $v$  from  $T$  to  $S$ . For example, if  $v$  is a split vertex, the counterclockwise ordering of its outgoing edges  $e_1, \dots, e_p$  is the same as their  $\preceq$  order; and in  $\preceq$  order these edges are all equivalent to  $v$ 's incoming edge  $e$ , in the sense that they have the same predecessors and successors. The concentration profile in  $e$  is divided into decreasing concentration profiles of  $e_1, \dots, e_p$ . With these observations, the inductive assumption applied to edges from  $S$  (which include  $e$ ) implies that both (cpm1) and (cpm2) are preserved. The argument for join nodes is similar. ◀

**Approximate concentration profiles.** In our technique, we approximate concentration profiles by simple 3-piece linear functions specified by four parameters  $a_L, a_R, d_L,$  and  $d_R$ , as shown in Figure 3. In interval  $[0, d_L]$  the concentration is  $a_L$ , in interval  $[w - d_R, w]$  the concentration is  $a_R$ , and the concentration linearly decreases in interval  $[d_L, w - d_R]$ , from  $a_L$  to  $a_R$ . Throughout the paper we will refer to such simplified profile functions as *SP-functions*. The value of  $w - d_L - d_R$  represents the diffusion length and is denoted  $L$ . The area under the profile curve, divided by the channel width, represents the concentration value  $c$ .

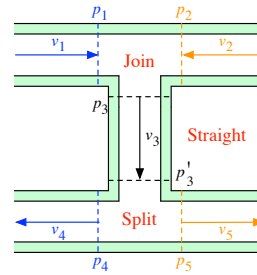
In Section 6 we explain how we can use SP-functions to compute approximate concentration profiles for each part of the grid design.

## 5 Computing Flow Rate and Pressure

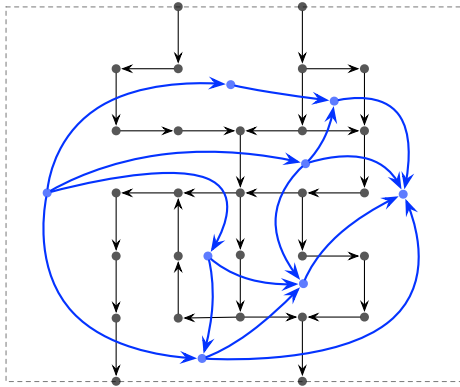
The computation of the flow direction, flow rate and pressure in each channel of the grid is quite straightforward, and it can be achieved by solving a system of linear equations. The unknowns are pressure values at every grid node and flow velocity in every channel. The



■ **Figure 3** Concentration profile SP-function.



■ **Figure 4** Grid partition



■ **Figure 5** Grid representation graph  $G$  (black) and its dual graph  $\tilde{G}$  (blue).

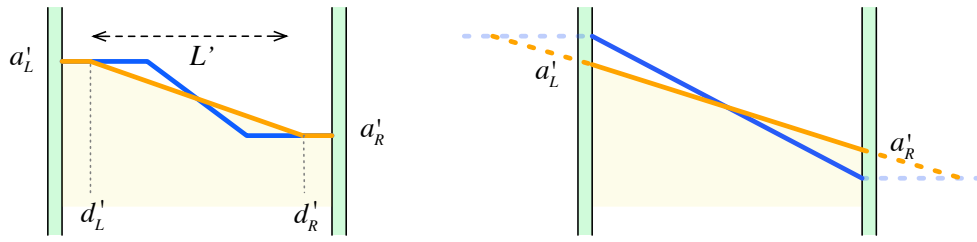
first set of equations in this system are flow conservation equations: at every grid node the total inflow is equal to the total outflow. The second set of equations are Hagen–Poiseuille equations which give relationship between the flow rate and the pressure drop between the two ends of a channel:  $\Delta P = QR$ , where  $Q$  is the volumetric flow, and  $R$  is the flow resistance. As the resistance value is the same in every channel segment and the input data specifies the velocity at the grid inlets, the exact value for  $R$  is not actually needed and can be assumed to be 1.

One thing to note is that in our setting we assume there is no friction at the walls of the channel, thus implying that the velocity is uniform across the channel, which simplifies the formulas for updating the profiles. (With friction, the velocity profile is a parabolic function.) We found, however, that this assumption has only a negligible effect on the computed concentration values.

## 6 Algorithm for Estimating Concentration Profiles

The core of our algorithm is a method for updating approximate concentration profiles (represented by SP-functions) along the grid, namely part (4) of the overall algorithm in Section 3. We describe this algorithm in this section.

As mentioned earlier in Section 3, the grid is partitioned into parts: straight channels and nodes, where nodes can be of several types depending on the flow directions of its channels: join nodes (2-way or 3-way), split nodes (2-way or 3-way), and combined join/split nodes (2 inflows and 2 outflows). This partitioning is illustrated in Figure 4. In this figure, the



■ **Figure 6** Updating the concentration profile in a straight channel in Case 1 (on the left) and Case 2 (on the right).

channels are cut at points  $p_1, p_2, p_3, p'_3, p_4$  and  $p_5$ , producing one join node, one straight channel, and one split node.

In the join node at the top, flows 1 and 2 are joined into flow 3. The concentration profile at point  $p_3$  is computed by combining SP-profiles at points  $p_1$  and  $p_2$ , taking the velocities into account. The combined function may not be an SP-function, and if so, we approximate it by an SP-function.

The straight channel stretches from the beginning of the channel at point  $p_3$  to its end point  $p'_3$ . The approximate SP-profile at point  $p'_3$  is computed from the SP-profile at point  $p_3$  using the diffusion formula.

In the split node at the bottom, we use the profile at point  $p'_3$  and the flow velocities to compute the profiles at points  $p_4$  and  $p_5$ . This case is relatively simple, as splitting an SP-function profile produces SP-functions, so no additional simplification is needed here.

## 6.1 Straight Channels

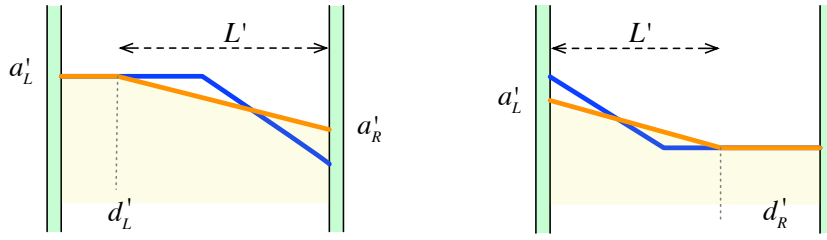
For a straight channel, the SP-profile changes over time with diffusion length increasing, that is with the middle portion of the profile function becoming gradually longer and flatter. The SP-profile may also change its form, with  $d_L$  becoming 0 or  $d_R$  becoming 0. We divide the evolution of the profile function along a straight channel into time intervals short enough so that in each such time interval the profile function has the same form.

We now demonstrate how the profile changes in a straight channel during one of these time intervals of length  $\Delta t$ . The fundamental idea behind our approach is this: we think of the current profile function as being a result of a mixing process, starting from a “pure” 1/0-valued profile, and lasting for some time  $t$ . This allows us to compute  $t$  from the diffusion length formula. Once we have  $t$ , we can compute the new profile function at time  $t + \Delta t$ , providing that  $\Delta t$  is small enough so that the form of the profile function does not change. This leads to a relatively simple solution for profiles whose step function has three non-empty segments; that is, when  $d_L > 0$  and  $d_R > 0$  in Figure 3 (Case 1 below). If  $d_L = 0$  or  $d_R = w$ , or both, a slightly less direct approach is required (Cases 2,3 and 4 below).

Case 1:  $d_L > 0$  and  $d_R > 0$  (see Figure 6). As indicated above, using formula (1) we compute  $t = L^2/4D$ . Next, we compute the new diffusion length  $L'$  after some  $\Delta t$ :  $L' = 2\sqrt{D(t + \Delta t)} = \sqrt{L^2 + 4D\Delta t}$ . This will give us the new concentration profile at time  $t' = t + \Delta t$ , defined by parameters  $d'_L = d_L - (L' - L)$  and  $d'_R = d_R - (L' - L)$ .

Case 2:  $d_L = 0$  and  $d_R = 0$  (see Figure 6). The channel boundaries introduce some distortion into the diffusion process that is difficult to model. Our approach here is based on the observation (verified experimentally) that this distortion has negligible effect on the overall profile. Thus we think about the current concentration profile as the linearly decreasing part





■ **Figure 7** Updating the concentration profile in a straight channel in Case 3 (on the left) and Case 4 (on the right).

of a concentration profile in a “virtual” wider channel in which the concentration profile has the same form as in Case 1, with  $L = w$ . Following the method from Case 1, we can compute the new virtual SP-profile with respect to this wider channel, and the new actual SP-profile is obtained as its section within the channel. (This section will always consist of only the sloped part.)

**Case 3:**  $d_L > 0$  and  $d_R = 0$  (see Figure 7). The new SP-profile in this case is computed based on the assumption that the value of  $d_L$  will decrease according to formula (1). This gives us the new value  $d'_L$  for the new SP-profile, namely  $d'_L = d_L - (L' - L)$  for  $L' = 2\sqrt{D(t + \Delta t)} = \sqrt{4D\Delta t + (w - d_L)^2}$ . Then we use the molecular preservation property (that is, that the area under the profile does not change) and straightforward calculation to obtain the new concentration at the right wall,  $a'_R = a_L + L(a_L - a_R)/L'$ .

**Case 4:**  $d_L = 0$  and  $d_R > 0$  (see Figure 7). This case is symmetric to Case 3, and similar calculation gives us the values of  $d'_R$  and  $a'_L$ .

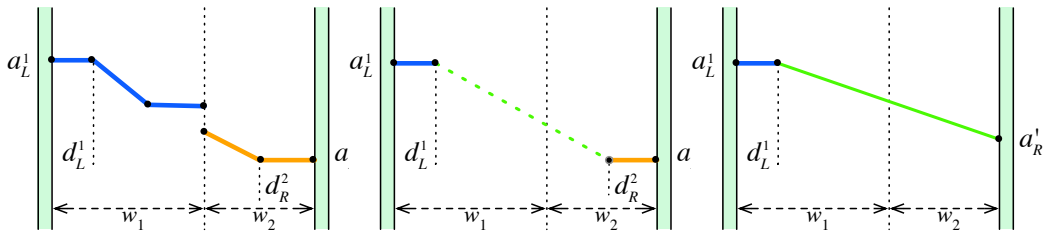
## 6.2 Joining Concentration Profiles

To join flows, we first simply combine together the SP-functions of two or three joined channels, with the portion of the channel width that each joined flow occupies being proportional to the velocities of the inflows, as shown in Figure 8. We will refer to this profile as the *combined profile*. In general, the combined profile will not be an SP-function. If this is the case, we will need to simplify it to an SP-function. This will be done in two steps. First we will convert the combined profile into a *tentative* SP-profile, which will be later adjusted to satisfy the reactant volume preservation property.

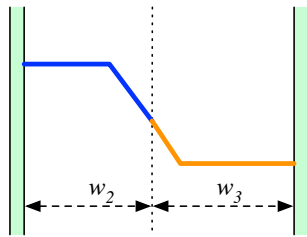
The correctness of profile joining depends critically on Theorem 1. This theorem implies that the concentration of the combined profile is non-increasing from left to right, as illustrated in Figure 8. This figure shows two profiles being combined. The case of combining three profiles is essentially the same, as the middle channel’s SP-function is only needed to compute the area under the combined function; its parameter can be ignored. Thus to simplify the description below, we will assume that we are dealing with a 2-way join node.

Let  $a_L^1$  and  $d_L^1$  represent the parameters of the combined profile inherited from the corresponding parameters of the left joined channel. (So  $a_L^1$  is the concentration along the left wall in the left channel, and  $d_L^1$  is the length of its SP-profile’s left flat segment, but rescaled according to the channel’s flow velocity.) By  $a_R^2$  and  $d_R^2$  we denote the corresponding parameters inherited from the right joined channel. We take these four values as the parameters of our *tentative* SP-function profile. This function is only tentative, because the area under this SP-function may be different than that under the combined profile.

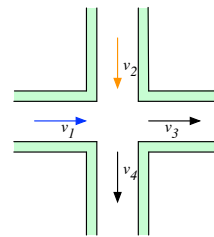
The final SP-profile, whose parameters will be denoted  $a'_L$ ,  $d'_L$ ,  $a'_R$  and  $d'_R$ , is computed



■ **Figure 8** Joining concentration profiles of two flows (blue and orange). Combined profile on the left. Tentative SP-profile in the middle. On the right, one possible final SP-profile in the case when the area under the combine profile is too small.



■ **Figure 9** Splitting concentration profiles



■ **Figure 10** A join-and-split node.

from the tentative SP-profile by adjusting it to make sure that the reactant volume (the area under the profile) is preserved. This is done as follows. Let  $A$  be the area under the original combined profile (before converting it into the tentative form). If the area under the tentative profile is smaller than  $A$ , then the left segment of the final profile is the same as in the tentative profile, that is  $a'_L = a_L^1$  and  $d'_L = d_L^1$ , while the middle and right segments are adjusted to increase the area to  $A$  as follows: We start with  $d'_R = d_R^2$  and  $a'_R = a_R^2$ . We then decrease  $d'_R$  until either the area becomes  $A$  or  $d'_R$  is reduced to 0. If  $d'_R$  becomes 0, we then increase  $a'_R$  until the area becomes  $A$ . The other case is when the area under the tentative profile is too large. This case is symmetric: the right segment of the final profile is the same as in the tentative profile, and we gradually lower the middle and left segment to reduce the area to  $A$ .

### 6.3 Splitting Concentration Profiles

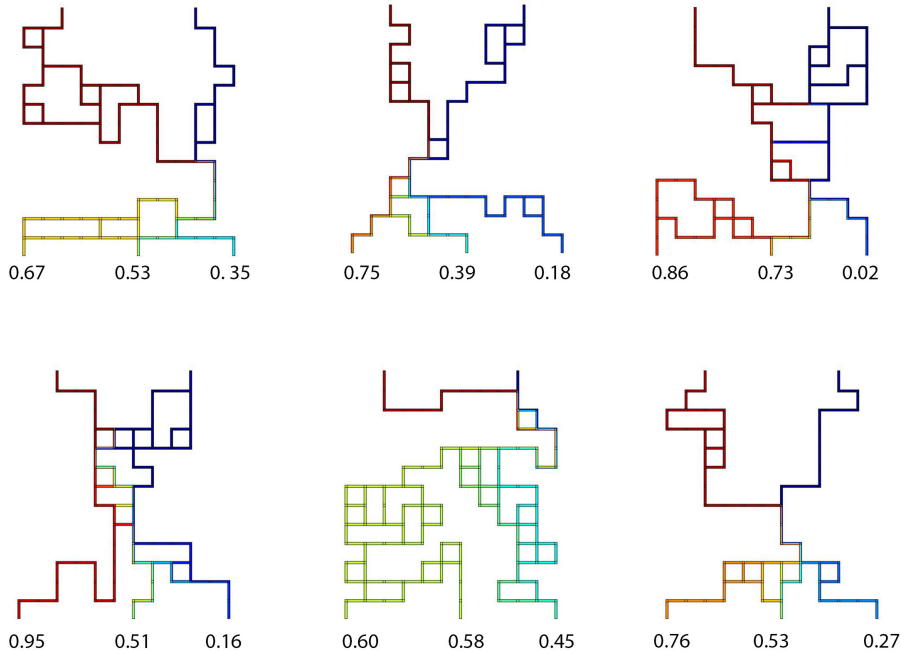
To split the flow at a node (either 2-way or 3-way), the split profiles are determined by dividing the profile of the inflow proportionally to the velocity ratios of the outflows (see Figure 9) and appropriate rescaling. Conveniently, splitting a profile represented by an SP-function produces profiles that are also in the same form, and the parameters of these new profiles can be determined with a straightforward computation. Thus in this case no further simplifications of the new profiles are needed.

### 6.4 Join-and-Split Nodes

In the grid there may also be nodes with two inflows and two outflows. This node must have the form shown in Figure 10, namely the inflow channels are adjacent, and so are the outflow channels. (The other option, with the two inflow channels being opposite of each other, is impossible, as this would imply the existence of flow circulation in the grid.)

We treat this case by first joining the two inflow SP-profiles, as discussed in Section 6.2, then splitting the combined SP-profile into two SP-profiles for the outflow channels, as discussed in Section 6.3.

## 7 Experimental Results

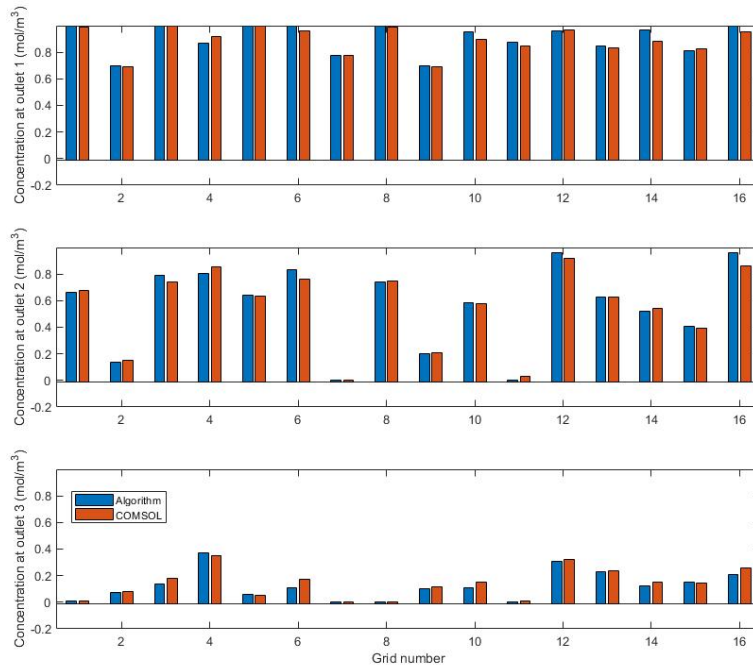


■ **Figure 11** Randomly constructed  $12 \times 12$  grids with concentration values at the outlets.

We used MATLAB® with COMSOL Multiphysics® via LiveLink™ [5] to generate our test grids. Note that in the method from [14] most generated chips have unreachable or “dead-end” channels, namely channels that do not appear on an inlet-to-outlet path. Such channels are redundant, as they have no effect on the mixing process. Our generator uses a similar approach as in [7] to generate only grids that are connected and have no redundant channels. Figure 11 shows six examples of random  $12 \times 12$  grids obtained from our generator as well as their outlets’ concentrations.

Our concentration prediction algorithm is implemented in Python and tested on a 3.50GHz quad core 32GB RAM workstation. We conducted an experimental comparison of our algorithm with a COMSOL simulation. In our experiments we used 200  $12 \times 12$  sample random grids (obtained from our generator) with two inlets and three outlets. For COMSOL simulations we used very fine triangular meshes that contained from 100,000 to 300,000 elements.

The results for fluid velocity at the 3 outlets are very consistent with COMSOL simulation, with the average percentage difference of velocity values of about 0.8%. For concentration values at the outlets, the average absolute difference is  $0.017 \text{ mol/m}^3$ , which is only 1.7% of maximum concentration. The maximum absolute difference is  $0.09 \text{ mol/m}^3$ .



■ **Figure 12** Comparison of concentration values at the outlets. Blue bars represent our algorithm and red bars represent COMSOL.

Figure 12 shows the difference of concentration values at 3 outlets between the algorithm and COMSOL, on 16 grid designs.

Execution times are measured on the same sample set of 200 grids. On average, COMSOL takes approximately 1.5 minutes to finish the computation of one  $12 \times 12$  grid. These times also vary significantly among different grids, with the fastest time of about 1 minute and the longest around 6 minutes. Our algorithm is several orders of magnitude faster, requiring on average only 0.0075 second to process one grid.

## 8 Discussion

In this work we show that fluid mixing in microfluidic grids can be efficiently simulated using simple 3-piece linear functions to model concentration profiles. Our algorithm is very fast, outperforming COMSOL simulations by several orders of magnitude, while producing nearly identical results.

To clarify, we should add that this algorithm is not necessarily meant as a complete substitute for COMSOL simulation. For example, in the application to populating mixing grid libraries in the approach from [14], one can apply our algorithm to select a collection of randomly generated designs with potentially useful concentration vectors, and then re-verify these designs with COMSOL. This way, COMSOL simulation will be performed only on a small fraction of generated grids, significantly improving the overall performance.

While our current implementation of the algorithm assumes that the input is a grid design, the overall technique applies to arbitrary acyclic planar graphs. The only required

assumptions involve inlets and outlets: all inlets and outlets must be located on the external face, cannot interleave, and the inlet concentrations must be non-decreasing in the clockwise direction along the external face. (This is not a significant restriction, as in a microfluidic device its inlets and outlets would normally be located along its edge.)

Another possible enhancement of our method is related to the assumption that the mixing process in microfluidic grids is exclusively caused by diffusion. While this assumption is valid for flows along straight channels, prior work in [1] showed that in reality convection generated in channel bends affects fluid mixing as well. (This observation will also likely apply to the split and join nodes.) Taking such convection effects into account can further improve the accuracy of our method.

---

## References

---

- 1 Nobuaki Aoki, Ryota Umei, Atsufumi Yoshida, and Kazuhiro Mae. Design method for micromixers considering influence of channel confluence and bend on diffusion length. *Chemical Engineering Journal*, 167(2-3):643–650, 2011.
- 2 Giuseppe Di Battista and Roberto Tamassia. Algorithms for plane representations of acyclic digraphs. *Theoretical Computer Science*, 61(2):175 – 198, 1988.
- 3 S. Bhattacharjee, B.B. Bhattacharya, and K. Chakrabarty. *Algorithms for Sample Preparation with Microfluidic Lab-on-Chip*. River Publishers Series in Biomedical Engineering. River Publishers, 2019.
- 4 S Bhattacharjee, S Poddar, S Roy, J Huang, and B Bhattacharya. Dilution and mixing algorithms for flow-based microfluidic biochips. *IEEE Transactions on Computer-Aided Design of Integrated Circuits and Systems*, 36(4):614–627, April 2017.
- 5 COMSOL, Inc. Comsol.
- 6 Stephen C. Jacobson, Timothy E. McKnight, and J. Michael Ramsey. Microfluidic devices for electrokinetically driven parallel and serial mixing. *Analytical Chemistry*, 71(20):4455–4459, 1999.
- 7 Weiqing Ji, Tsung-Yi Ho, and Hailong Yao. More effective randomly-designed microfluidics. *2018 IEEE Computer Society Annual Symposium on VLSI (ISVLSI)*, 2018.
- 8 Kim Jungkyu, Johnson Michael, Hill Parker, and Gale Bruce. Microfluidic sample preparation: cell lysis and nucleic acid purification. *Integrative Biology*, 1:574–586, Oct 2009.
- 9 Athina S. Kastania, Katerina Tsougeni, George Papadakis, Electra Gizeli, George Kokkoris, Angeliki Tserepi, and Evangelos Gogolides. Plasma micro-nanotextured polymeric micro-mixer for dna purification with high efficiency and dynamic range. *Analytica Chimica Acta*, 942:58–67, 2016.
- 10 Brian J. Kirby. *Micro- and nanoscale fluid mechanics: transport in microfluidic devices*. Cambridge University Press, 2013.
- 11 Brian M. Paegel, William H. Grover, Alison M. Skelley, Richard A. Mathies, and Gerald F. Joyce. Microfluidic serial dilution circuit. *Analytical Chemistry*, 78(21):7522–7527, 2006. PMID: 17073422.
- 12 Todd M. Squires and Stephen R. Quake. Microfluidics: Fluid physics at the nanoliter scale. *Rev. Mod. Phys.*, 77:977–1026, Oct 2005.
- 13 Roberto Tamassia and Ioannis G. Tollis. A unified approach to visibility representations of planar graphs. *Discrete & Computational Geometry*, 1(4):321–341, Dec 1986.
- 14 Junchao Wang, Philip Brisk, and William H. Grover. Random design of microfluidics. *Lab Chip*, 16:4212–4219, 2016.
- 15 Paul Yager, Thayne Edwards, Elain Fu, Kristen Helton, Kjell Nelson, Milton R. Tam, and Bernhard H. Weigl. Microfluidic diagnostic technologies for global public health. *Nature News*, Jul 2006.